


FULL PAPER

Investigation of plasma-induced chemistry in organic solutions for enhanced electrospun PLA nanofibers

Fatemeh Rezaei¹  | Yury Gorbanev² | Michael Chys³ | Anton Nikiforov¹ |
Stijn W. H. Van Hulle³ | Paul Cos⁴ | Annemie Bogaerts² | Nathalie De Geyter¹

¹ Faculty of Engineering and Architecture, Department of Applied Physics, Research Unit Plasma Technology (RUPT), Ghent University, St-Pietersnieuwstraat 41 B4, 9000 Ghent, Belgium

² Department of Chemistry, Research group PLASMANT, University of Antwerp, Universiteitsplein 1, 2610 Wilrijk, Belgium

³ LIWET, Department of Industrial Biological Sciences, Ghent University Campus Kortrijk, Graaf Karel de Goedelaan 5, B-8500 Kortrijk, Belgium

⁴ Department of Pharmaceutical Sciences, University of Antwerp, Universiteitsplein 1, 2610 Wilrijk, Belgium

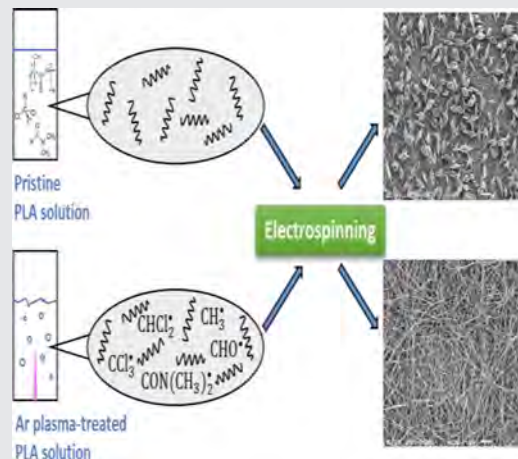
Correspondence

Fatemeh Rezaei, Faculty of Engineering and Architecture, Department of Applied Physics, Research Unit Plasma Technology (RUPT), Ghent University, St-Pietersnieuwstraat 41 B4, 9000 Ghent, Belgium.
Email: fatemeh.rezaei@UGent.be

Funding information

Fonds Wetenschappelijk Onderzoek, Grant number: G.0379.15N; FP7 Ideas: European Research Council, Grant number: 335929 (PLASMATS); European Marie Skłodowska-Curie Individual Fellowship "LTPAM", Grant number: 657304

Electrospinning is a versatile technique for the fabrication of polymer-based nano/microfibers. Both physical and chemical characteristics of pre-electrospinning polymer solutions affect the morphology and chemistry of electrospun nanofibers. An atmospheric-pressure plasma jet has previously been shown to induce physical modifications in polylactic acid (PLA) solutions. This work aims at investigating the plasma-induced chemistry in organic solutions of PLA, and their effects on the resultant PLA nanofibers. Therefore, very broad range of gas, liquid, and solid (nanofiber) analyzing techniques has been applied. Plasma alters the acidity of the solutions. SEM studies illustrated that complete fiber morphology enhancement only occurred when both PLA and solvent molecules were exposed to pre-electrospinning plasma treatment. Additionally, the surface chemistry of the PLA nanofibers was mostly preserved.



KEYWORDS

atmospheric pressure plasma, electrospun nanofibers, EPR, OES, pre-electrospinning plasma treatment

1 | INTRODUCTION

In recent years, the chemical processes induced in liquids by non-thermal atmospheric pressure plasmas have been extensively investigated due to the high potential of plasma in a wide variety of applications including synthetic chemistry.^[1–3] The mechanisms of plasma-liquid interactions are investigated by many research groups because they present paramount importance in systems with liquid

solutions.^[1,3,4] A very novel application of this promising research field is the use of non-thermal plasma technology for the treatment of pre-electrospinning polymer solutions.^[5–9]

Electrospinning is well known as a cost-effective and versatile technique for the fabrication of polymer-based nano/micro fibers.^[10] Such synthetic and natural polymeric nanofibrous mats are of great interest for biomedicine, biotechnology, and industry.^[11–15] By varying polymer type and electrospinning processing conditions, nanofibers can be

spun with a large surface area for different potential applications such as membranes for biological and/or chemical sensors,^[16] wound healing,^[17] drug delivery,^[18] and tissue engineering.^[19] Several processing parameters determine the morphology of the resultant nanofibers, e.g., the electrospinning working parameters, the properties of the electrospinning polymer solution, and ambient conditions.^[8,20] Besides selecting the right working parameters, preparation of a polymer solution with suitable characteristics is also very important in the electrospinning process. Several research groups have described the influence of electrospinning working parameters (e.g., applied voltage, feed rate, and working distance) and the solution physical properties (e.g., conductivity, surface tension, and viscosity) on the morphology of electrospun nanofibers for numerous polymer solutions.^[20–22] However, the effects of physical/chemical treatments of polymer solutions prior to the electrospinning process in an effort to improve electrospinnability have not been widely studied. A few methods including the addition of different salts to the polymer solutions^[23–25] and using physical cross-linkers^[26] have been reported to enhance the electrospinnability of polymer solutions. However, these methods often involve additional costs, safety, and environmental concerns.^[27] An efficient, environmentally benign, and non-toxic method to improve the electrospinnability of polymer solutions is thus required.

Recently, pre-electrospinning plasma treatment (PEPT) has been shown to improve the electrospinnability of different polymer solutions.^[5–7,9,28] PEPT has been found to enhance the electrospinnability, and helped obtaining thinner and bead-free nanofibers at significantly lower polymer concentrations.^[5–9,28] However, further research is required as attention has been mostly paid to examining the nanofibers without a detailed investigation of the gas phase plasma and the plasma-induced changes in the liquid solvents. To elucidate some of the multiple remaining questions on PEPT, this study examines the resultant electrospun nanofibers, and aims to unravel the occurring plasma-liquid interactions. As a target polymer in our work, polylactic acid (PLA) was chosen. PLA is a biodegradable aliphatic polyester derived from lactic acid, a naturally occurring organic acid. This biocompatible and non-toxic polymer has been extensively used in various biomedical fields such as tissue engineering, wound healing, and drug delivery systems,^[29] i.e., fields where PLA nanofibers play an important role.

In agreement with the results of other researchers,^[6,7] we previously reported^[8] that the viscosity and electrical conductivity of PLA solutions increased considerably after PEPT with an argon plasma jet generated directly in the polymer solution. In addition, the effects of various operational plasma parameters such as, plasma treatment time, argon flow rate, applied voltage, and polymer concentration, on the viscosity, surface tension, and electrical

conductivity of PLA solutions were studied in detail. We showed that the increased viscosity and conductivity induced by PEPT positively affected the electrospinnability of PLA and the morphology of the resultant PLA nanofibers. The question that remains up to now is which plasma-induced chemical species are responsible for the observed increase in viscosity and conductivity. It is also yet unclear whether the PLA polymer chains themselves undergo some changes during PEPT, or the observed results are caused exclusively by the plasma-induced changes to the solvent molecules.

To gain more knowledge on the effects of PEPT, the plasma-induced chemical changes to both PLA solutions and pure organic solvents are investigated in this work. An atmospheric-pressure plasma jet directly submerged into the liquid was used. The plasma species generated in the plasma jet afterglow operating in ambient air and submerged in the solutions were determined using optical emission spectroscopy (OES) for various plasma operational conditions. pH measurements were performed before and immediately after each PEPT to investigate whether the performed plasma treatments induce some changes to the acidity of the examined liquids. In addition, the plasma-induced chemical changes in pure solvents as well as in PLA solutions were investigated in detail via fluorescence excitation-emission matrix (EEM) spectroscopy, UV–Vis absorption spectroscopy, nuclear magnetic resonance (NMR) spectroscopy, and electron paramagnetic resonance spectroscopy (EPR). EPR was used to detect and identify the species generated in the examined plasma-treated liquids. Besides liquid characterization, a morphological, and chemical evaluation of the resultant electrospun nanofibers was carried out using scanning electron microscopy (SEM) and X-ray photoelectron spectroscopy (XPS), respectively. This broad set of characterization techniques enabled obtaining information about the fundamental processes occurring during PEPT.

2 | MATERIALS AND METHODS

Biodegradable PLA granules $(C_3H_4O_2)_n$ with molecular weight of $\approx 230,000 \text{ g mol}^{-1}$ were purchased from Goodfellow. Chloroform (CHL $[CHCl_3]$; 99.5%) and N,N-dimethylformamide (DMF $[C_3H_7NO]$; 99.8%) were purchased from Sigma–Aldrich. All chemicals and solvents were used as received.

To prepare PLA solutions with PLA concentrations of 4, 5, and 6% w/v, 0.4, 0.5, and 0.6 g of PLA was dissolved in 10 mL of a binary solvent mixture of CHL:DMF with a volume ratio of 8:2. Transparent and homogenous PLA solutions for plasma modification and/or electrospinning were obtained after sufficient stirring.

PEPT of the prepared PLA solutions was performed with an atmospheric-pressure plasma jet, as shown in Figure 1a.

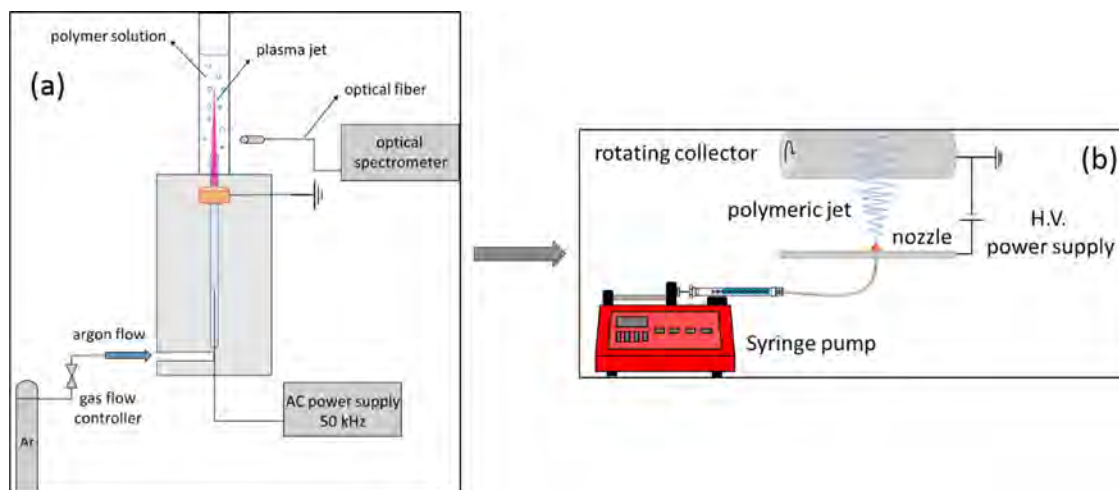


FIGURE 1 Schematic representation of (a) the atmospheric-pressure argon plasma jet for PEPT, and (b) the electrospinning device

The argon plasma jet was composed of a cylindrical quartz tube (inside and outside diameters of 1.5 and 3 mm, respectively and 130 mm long) and an aluminum rod as high-voltage electrode, which was embedded inside the quartz tube. The quartz tube was covered by a Teflon shell (which was a hollow cylinder with inside and outside diameters of 13 and 62 mm, respectively) and was aligned along the central axis of this Teflon cylinder. The high-voltage electrode was connected to a 50 kHz sinusoidal customer-made power supply with maximum output voltage and power of 25 kV (peak to peak) and 500 W, respectively. ($\varnothing = 13$ mm, thickness = 10.5 mm) was fixed 18 mm away from the tip of the high-voltage pin electrode and serves as a ground electrode. The distance between the bottom of the copper ring and the end of the capillary is 40 mm. Argon (Air Liquid, purity >99.999%) was used as carrier gas in this work and the gas flow rate through the capillary was controlled by a mass flow controller (Model: F-201CV, Bronkhorst, Netherlands). The sample holder for polymer solutions was a quartz tube with an inner and outer diameter of 17.5 and 22.5 mm, respectively which was placed around the high end of the plasma jet quartz tube. Prior to plasma modification, the quartz sample holder is filled with 10 ml of the PLA solution and this volume is kept constant in all experiments. As such, the liquid height in the quartz sample holder was each time approximately 40 mm. In this work, PEPTs were carried out with various plasma exposure times (1–9 mins), various Ar gas flow rates ($0.3\text{--}1.1\text{ L min}^{-1}$), and various applied voltage amplitudes (1.6–2.1 kV), the latter one resulting in a discharge power varying from 1.6 to 2.0 W.

Electrospinning of PLA solutions was performed immediately after each PEPT in a bottom-up configuration (Nanospinner 24, Inovenso, Turkey), as schematically shown in Figure 1b. Prior to electrospinning, the pristine and plasma-treated PLA solutions were put in a 10 mL plastic syringe, which was then installed in a syringe pump (NE-300 Just

Infusion™ syringe pump) which controls the flow rate of the polymer solution through a polyethylene tube (inner diameter of 2 mm) ending in an aluminum feeding pipe containing a single brass nozzle with an inner diameter of 0.8 mm. During the electrospinning process, the polymer flow rate is maintained at 1 mL h^{-1} . The brass nozzle is vertically placed below a stainless steel drum collector rotating at 100 rpm at a distance of 17.5 cm. During the electrospinning process, a DC high voltage of 23 kV is applied to the nozzle, while the cylindrical collector is grounded. In this work, nanofibers are directly collected on an aluminum foil covering the rotating drum and the electrospinning process was carried out at ambient temperature with a relative humidity varying between 50% and 60%. To remove traces of residual chloroform or DMF in the electrospun nanofibers which can have potential toxic effects in biomedical applications, the electrospun materials were placed in a vacuum oven overnight before further processing.

3 | ANALYSES

To gather information on the excited radiative species generated in the plasma, optical emission of the argon plasma jet, sustained in ambient air as well as submerged in the PLA solutions, was monitored perpendicular to the axis of the plasma jet. This was done using an optical spectrometer (Ocean Optics, ADC1000-USB) with a low spectral resolution of 0.7 nm in the wavelength range 200–900 nm. To detect the optical emission spectra of the plasma jet afterglow (i.e., the part of the plasma jet that is in direct contact with the polymer solutions), an optical fiber was placed at 4.5 mm from the end of the capillary tube, as schematically shown in Figure 1a.

To investigate the changes in the plasma-treated media and the plasma-generated organic fragments in the liquid

phase, the pristine, and plasma-modified PLA solutions were subjected to EEM fluorescence spectroscopy. EEM fluorescence spectra were recorded using a Shimadzu RF-5301 fluorescence spectrophotometer equipped with a 150 W Xenon lamp as light source. EEM analysis was conducted with slit widths set at 5 nm for excitation (Ex) and emission (Em) modes. The Ex and Em sampling intervals were both set at 1 nm. In all EEM images shown in this work, the X-axis represents Em wavelengths ranging from 280 to 600 nm, and the Y-axis represents Ex wavelengths ranging from 220 to 450 nm. The EEM spectrum of distilled water was first determined and subtracted from all measured EEM spectra to remove interfering signals of first- and second-order Raman scattering using an interpolation technique. In the next step, the fluorescence intensity was corrected for the inner-filter effect using UV-Vis absorbance spectra (Shimadzu UV-1800, Japan) in the wavelength range 200–800 nm. Finally, the obtained fluorescence intensity was converted into Raman Units (R.U.) to remove instrument-dependent factors and the final EEM data were interpreted using the Parallel Factor (PARAFAC) technique.^[30]

Electrical conductivity and pH values of the PLA solutions were determined using a Mettler Toledo FiveEasy conductivity meter and a FiveEasy Plus pH meter, respectively. The pH probe used in this work is an InLab Science Pro-ISM pH probe specifically designed to determine pH values in organic solvents. Moreover, the solution viscosity was measured using a Brookfield DV2T EXTRA viscometer operating at room temperature. All measurements were repeated at least three times.

UV-Vis spectroscopy was applied to investigate the optical differences between untreated and plasma-treated solutions. The measurements were performed in the liquid samples on a Thermo Fisher Genesys 6 spectrophotometer. Quartz cuvettes (Hellma) were used with a 10 mm path length and a 2 mm internal width.

The detection of the radical species in the plasma-treated solutions was done by EPR. EPR spectra were recorded using a Magnetech MiniScope MS200 spectrometer operating with the following parameters: frequency 9.4 GHz, modulation amplitude 0.1 mT, power 3.16 mW, modulation frequency 100 kHz, sweep time 40 s, time constant 0.1, sweep width 10 mT, number of scans 3. In a typical experiment, a spin trap was added to the studied solution in a 100 mM concentration. 5-Dimethyl-1-pyrroline *N*-oxide (DMPO; Sigma-Aldrich, $\geq 97\%$) and *N*-tert-butyl- α -phenylnitron (PBN; Sigma-Aldrich, $\geq 97\%$) were used as spin traps for EPR spectroscopy. After PEPT, 50 μ L samples were immediately contained in glass capillaries (Hirschmann) and analyzed by EPR. The total time between plasma exposure and recording of the spectra was 1 min. The reported concentration values were obtained via double integration of the respective combined simulated spectra of the radical adducts. The quantitative calibration of the

EPR was performed with solutions of a stable nitroxide radical 4-hydroxy-2,2,6,6-tetramethylpiperidine-1-oxyl (4-hydroxy-TEMPO; Sigma-Aldrich, 98%) in a range of concentrations 1–100 μ M. The simulations of the EPR spectra were performed using a NIEHS P.E.S.T. WINSIM ver. 0.96. The hyperfine values used in the simulations were obtained from available literature.^[31]

NMR spectroscopy was used to study possible changes in the chemical composition of plasma-treated PLA solutions. ^1H and ^{13}C NMR spectra of the solutions were recorded in D_2O and/or CDCl_3 on a Bruker DRX-400 instrument, operating at 400 MHz and 100 MHz for ^1H and ^{13}C NMR, respectively.

The generated solid PLA nanofibers obtained after electrospinning were also characterized. The elemental surface composition of the PLA nanofibers was evaluated by XPS on a PHI Versaprobe II spectrometer employing a monochromatic Al K_α X-ray source ($h\nu = 1486.6$ eV) operating at 51.3 W. The pressure in the analyzing chamber was kept below 10^{-6} Pa during analysis and the photoelectrons were detected with a hemispherical analyzer positioned at an angle of 45° with respect to the normal of the sample surface. Survey scans and individual high resolution spectra (C1s and O1s) were recorded with a pass energy of 187.85 and 23.5 eV, respectively. Elements present on the PLA nanofiber surfaces were identified from XPS survey scans, which were obtained at 5 different locations per sample and quantified with Multipak 9.3.0 software using a Shirley background and applying the relative sensitivity factors supplied by the manufacturer of the instrument. Multipak was also applied to curve fit the high-resolution C1s peaks after the hydrocarbon component of the C1s spectrum (285.0 eV) was used to calibrate the energy scale. The peaks were further deconvoluted using Gaussian-Lorentzian peak shapes and the full-width at half maximum (FWHM) of each line shape was constrained below 1.8 eV.

The morphology of the electrospun PLA nanofibers was also examined using a JEOL InTouch Scope JSM-6010 SEM device. SEM images were taken (accelerating voltage of 7 kV and a working distance of 11 mm) after sputter-coating the samples with a thin layer of gold with a JEOL JFC-1300 Auto Fine Coater.

4 | RESULTS AND DISCUSSION

4.1 | Plasma diagnostics

As the first step of this study, the used atmospheric-pressure argon plasma jet was characterized by OES. Optical emission spectra were obtained to monitor the excited species present in the plasma jet afterglow sustained in ambient air and submerged in PLA solutions or pure solvents. Figures 2a and 2b show the optical emission spectra of the argon plasma jet

afterglow operating in ambient air and submerged in a 4% w/v PLA solution, respectively. The spectra are presented at the same intensity scale (in a.u.) to show the changes in transition line intensity.

As seen in Figure 2a, multiple transition lines were observed in the optical emission spectrum of the plasma jet afterglow operating in ambient air. An intense OH rotational band ($X^2\Pi_g \leftarrow A^2\Sigma^+$) at 308.49 nm and strong atomic argon emission lines ($4s \leftarrow 4p$) in the range 690–853 nm can be clearly observed. Some low intensity emission lines are however also present as can be seen in the inset of Figure 2a: emission due to the N_2 second positive system ($B^3\Pi_g \leftarrow C^3\Pi_u$) at 330–380 nm, a small emission line due to the N_2^+ first negative system ($X^2\Sigma_g^+ \leftarrow B^2\Sigma_u^+$) centered at 388 nm, emission attributed to atomic oxygen ($3s^5S \leftarrow 3p^5P$) at 777.53 nm, and emission due to the presence of NO radicals ($X^2\Pi \leftarrow A^2\Sigma^+$) at 282.87 nm.^[32–37] The identified nitrogen-containing components were most likely due to diffusion of ambient air into the plasma jet afterglow. The OH emission peak is probably caused by fragmentation of H_2O molecules which diffuse from ambient air to the plasma jet afterglow, while the atomic oxygen emission peak can result from H_2O fragmentation or O_2 dissociation.^[8,37] When the plasma jet was operated in a PLA solution (Figure 2b), the normalized intensity of the argon emission lines increased, while the

intensity of the OH band considerably decreased. The OH signal is possibly coming from the H_2O impurities in the gas and/or solvents. The observed intensity changes in the atomic argon emission lines in the plasma-solution system could be due to changes in the electron energy distribution.^[38] Additional transition lines from carbon fragments were present in the optical emission spectrum of the plasma-solution system: a CH band ($X^2\Pi \leftarrow B^2\Sigma^-$ and $X^2\Pi \leftarrow A^2\Delta$) at 386.89 and 431.19 nm, respectively, and the Swan system of C_2 lines ($X^3\Pi_u \leftarrow A^3\Pi_g$) at 473.5, 516.29, 558.11, and 563.26 nm.^[37,39–41] In addition, low intensity emission lines are also present, as can be seen in the inset of Figure 2b: a CN band ($X^2\Sigma^+ \leftarrow B^2\Sigma^+$) at 416.13 nm, an NH band ($X^3\Sigma^- \leftarrow A^3\Pi$) at 336.52 nm, and an Ar line ($1s_4 \leftarrow 3p_5$) at 419.72 nm.^[42–44] The presence of these additional transition lines suggests that PLA solution components (PLA polymer chains and/or solvent molecules) were possibly partially fragmented by the argon plasma jet during PEPT.^[37,39,40,45]

Since the main differences between the two emission spectra depicted in Figure 2 are observed in the wavelength range 250–600 nm, only this wavelength range will be examined in the rest of this section to elucidate the influence of various operational conditions on the excited species present in the plasma jet afterglow sustained in PLA solutions.

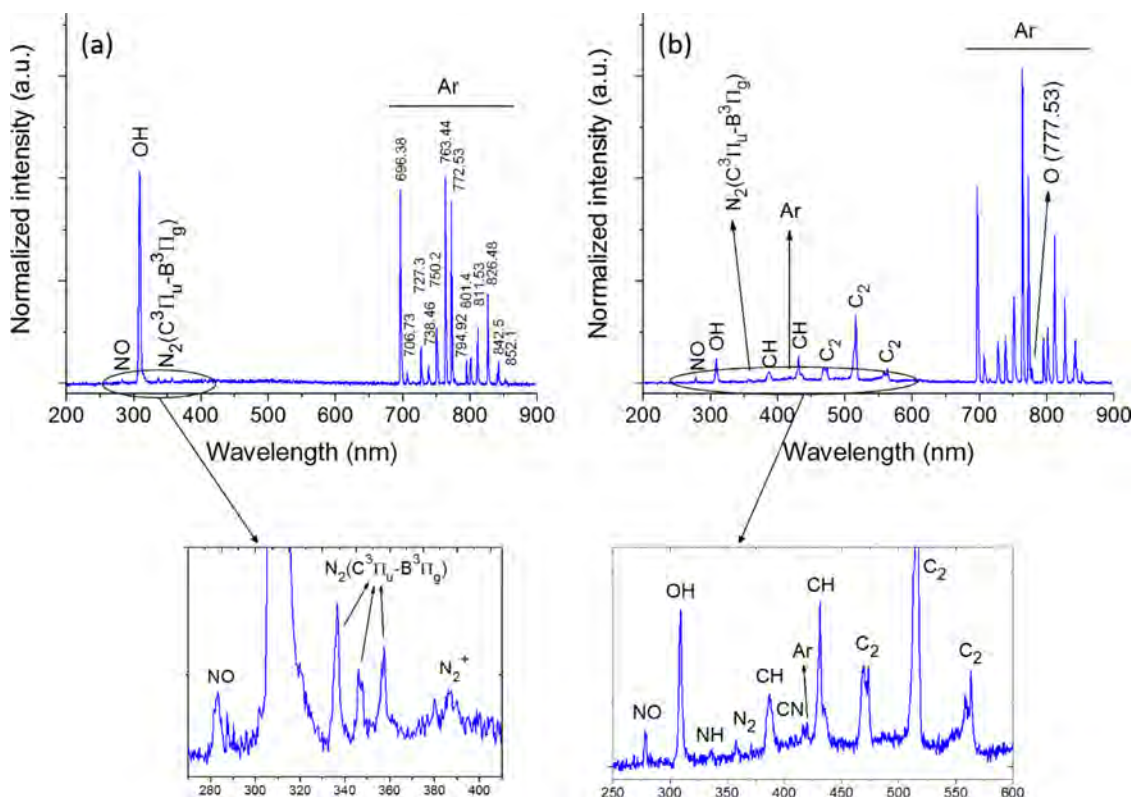


FIGURE 2 OES spectra of the atmospheric-pressure argon plasma jet afterglow (a) in ambient air and (b) submerged in a 4% w/v PLA solution (PEPT parameters: 5 min, 2 kV, 0.5 L min^{-1})

The OES spectra obtained during PEPT of pure CHL, pure DMF, the binary mixture of CHL:DMF, and PLA solutions with different polymer concentrations are presented in Figure 3. It is clearly seen from the data that the plasma jet afterglow sustained in pure CHL or pure DMF did not exhibit any significant peak emission in the examined wavelength range. A noticeable change however occurred when a mixture of both solvents was used, when transition lines from solution fragments appear in the spectrum (Figure 3a). This suggests that both CHL and DMF molecules need to be present in the solution before plasma-induced modification of solvent molecules occurs. The OES spectra of solutions with different PLA concentrations (Figure 3b) show that the same transition lines as in the binary solvent mixture were still present when PLA was added. However, the intensities of all transition lines in the studied wavelength region (250–600 nm) decreased with increasing PLA concentration. It is well known that increasing polymer concentration leads to an increase in solution viscosity.^[46–48] As a result of this higher viscosity, the gas bubbles generated in the solution during PEPT become smaller and therefore the intensity of the complete emission spectrum decreases with increasing PLA concentration. Due to this fact, most of the liquid characterization experiments in this work will be performed with a low PLA concentration solution (2% w/v) to avoid masking of obtained signals by PLA molecules. We note that even at this reduced concentration, the effect of PLA presence in the solutions could still be seen.

Figure 4 shows the effect of argon flow rate and applied voltage on the OES spectra of the plasma jet afterglow operating in ambient air and submerged in a 6% w/v PLA solution. In the plasma-solution system, unlike ambient air (Figures 4a and 4c), the increased gas flow rate and applied voltage caused a reduction in OH intensity.

At the same time, a strong increase in the intensity of emission lines of organic fragments (Figures 4b and 4d) and

argon (not shown) was observed with increased gas flow rate and increased applied voltage. This was as expected: higher voltage and gas flow rate (i.e., higher energy deposited into plasma generation) resulted in larger amounts of excited argon atoms and free electrons in the plasma-solution environment. Larger number of these species interacting with the molecules of the solvents result in a higher effective collision frequency between them, and thus effective chemical bond cleavage and higher fragmentation.

The effect of plasma treatment time on the optical emission of the plasma jet afterglow sustained in a 6% w/v PLA solution is presented in Figure S1 in the Supporting Information. Increasing plasma treatment time led to a strong reduction in the emission intensity of OH radicals, and at the same time to a strong increase in the intensity of emission lines from the organic fragments in the solutions. As these were the same trends as for the influence of voltage and gas flow, the same hypothesis can be used to explain these phenomena.

4.2 | EEM fluorescence and UV–Vis absorption spectroscopies, and pH measurements

Standardized EEM spectra of the pristine and plasma-modified liquids were obtained, providing information on the location and intensity of fluorescence peaks and distribution of fluorescence over different EEM regions. Figure 5 shows the EEM spectra of pure CHL, pure DMF, the binary mixture of CHL:DMF, and PLA solutions with various PLA concentrations before and after PEPT. The figures within contour lines in Figure 5 are the distribution of fluorescence intensity of each Ex-Em wavelength pair. The figures contained within the inner contour lines are of higher fluorescence intensity than the outer ones.

As can be seen in Figure 5, considerable plasma-induced changes in fluorescence were observed for the binary mixture of

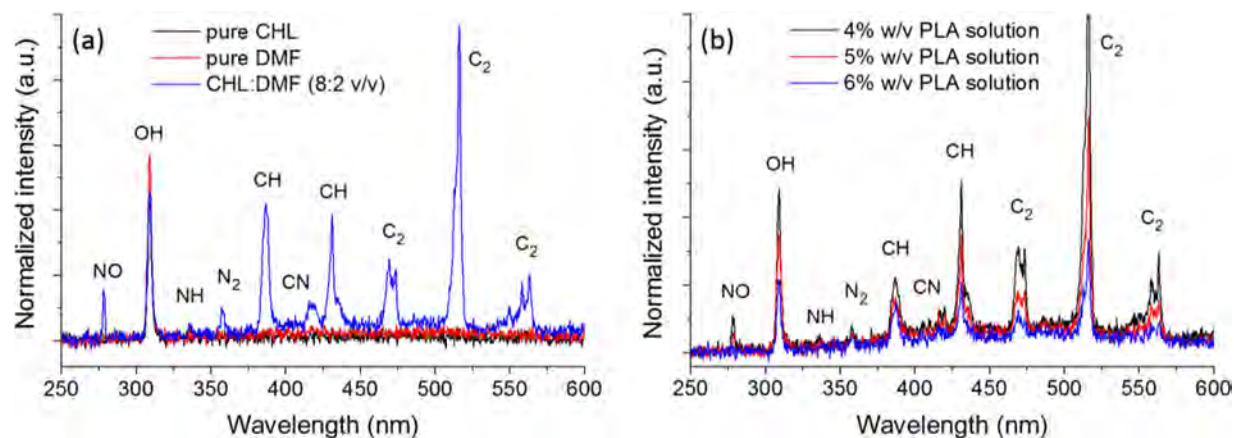


FIGURE 3 Optical emission spectra of the plasma jet afterglow sustained in (a) pure solvents and the solvent mixture used in this work and (b) PLA solutions with various concentrations (PEPT parameters: 5 min, 0.5 L min⁻¹, 2 kV)

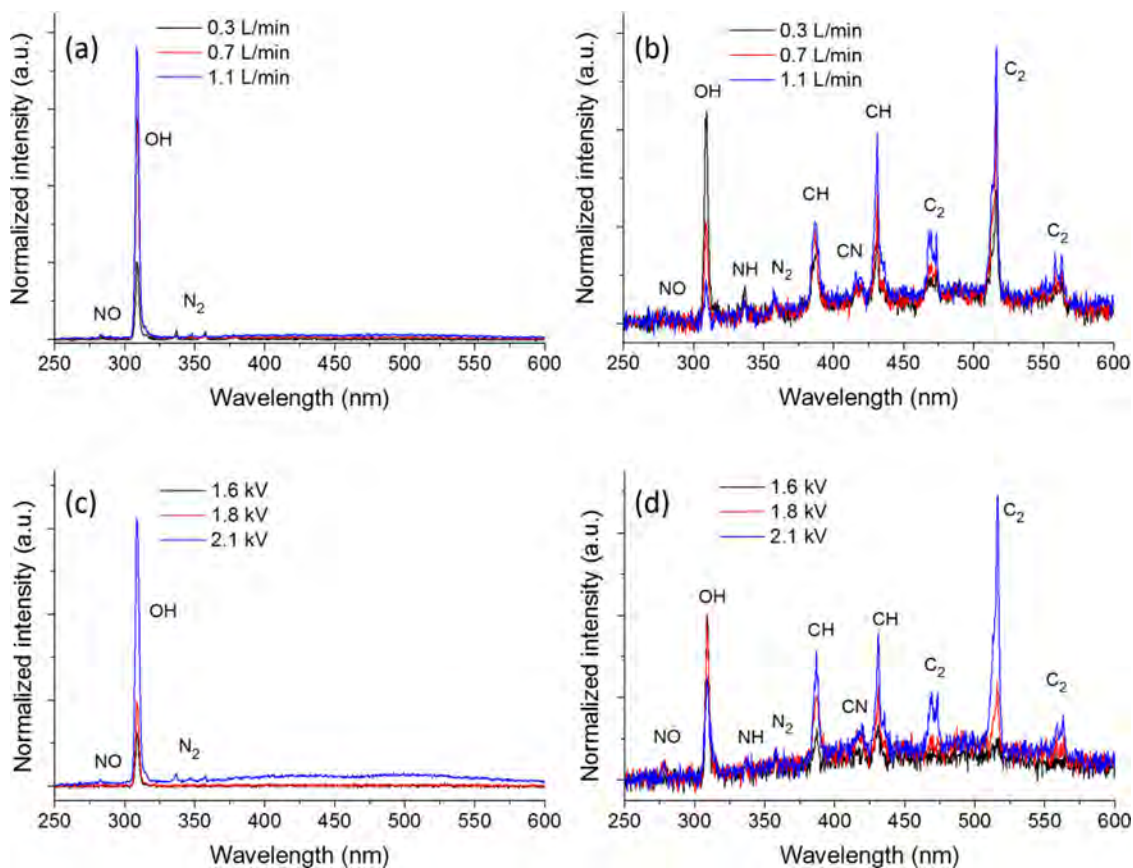


FIGURE 4 Optical emission spectra of the argon plasma jet afterglow as a function of gas flow rate (a) operating in ambient air and (b) submerged in a 6% w/v PLA solution (PEPT parameters: 5 min, 2 kV) and optical emission spectra of the argon plasma jet afterglow as a function of applied voltage (c) operating in ambient air and (d) submerged in a 6% w/v PLA solution (PEPT parameters: 5 min, 0.5 L min⁻¹)

CHL:DMF (8:2 v/v) after PEPT, but not in case of the pure CHL and DMF fluorescence spectra. These observations are in excellent agreement with the OES results shown in the previous section where no excited solvent fragments could be observed for the pure solvents. Untreated CHL shows a small fluorescence peak at Ex-Em of 250–507 nm, with only a small peak appearing after PEPT at Ex-Em of 365–412 nm. Both untreated and plasma-treated DMF show a fluorescence peak at Ex-Em of 290–295 nm. In the binary solvent mixture, the CHL peak does not shift, while there is a shift in the DMF peak towards higher Ex-Em values. The shift of the DMF peak towards longer excitation wavelengths may be attributed to the production of some oxygen-containing groups in the binary solvent mixture due to the presence of DMF.^[49] Also, the shift of this peak towards longer emission wavelengths can be related to assembly of the DMF molecules into larger molecules and consequently producing new organic compounds in the mixture.^[50] Both of these shifts indicate the intramolecular electron charge-transfer interactions between the molecules in the binary solvent mixture.^[51] Therefore, this intramolecular structure change leads to a different photochemical behavior.

After PEPT, the relative intensity of the CHL peak in the plasma-treated binary solvent mixture increases, while the

relative intensity of the DMF peak slightly decreases. These observations suggest that in the binary mixture CHL degraded more than DMF, resulting in larger conformational changes which expose fluorescent parts of the plasma-treated CHL molecules and hide them for the plasma-treated DMF molecules.^[49,50] Therefore, it would be expected that in the plasma-treated binary solvent mixture, the pH changes (will be shown in the next paragraphs) was mostly due to the plasma-treated CHL molecules, since the fluorescence intensities are highly sensitive to pH.^[49] At the same time, PEPT leads to a considerable broadening effect on the DMF peak in the binary solvent mixture. Also the shape of the contour plots of this peak changed from narrow ellipse to an irregular shape after PEPT. These observations could be related to the presence of plasma-generated chemicals in the binary solvent mixture.^[52]

The effect of increasing PLA concentration in the solutions from 4% to 6% w/v is also represented in Figure 5. The untreated PLA solutions in all cases exhibited a major peak located at Ex-Em of 275–388 nm (peak I), which can be attributed to the presence of PLA, as the relative intensity of this peak increases with increasing polymer concentration in the solutions. After PEPT, there is no shift in the position of peak I, but its relative intensity decreased after PEPT

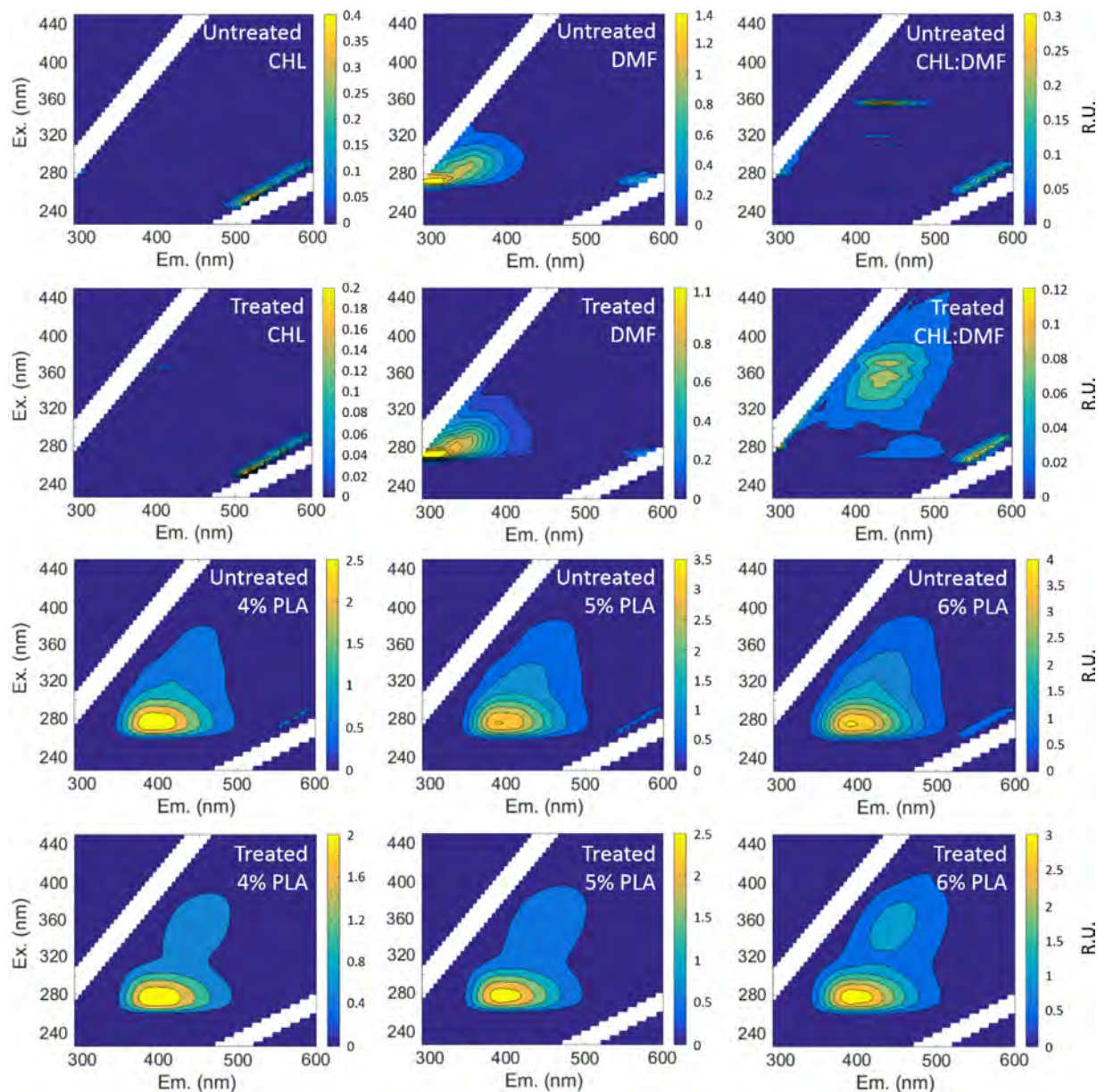


FIGURE 5 EEM spectra of pure solvents, the solvent mixture used in this work and PLA solutions with different PLA concentrations in the binary solvent mixture before and after PEPT (PEPT parameters: 2 kV, 0.5 L min⁻¹, 5 min)

for all examined PLA concentrations. Additionally, the EEM spectra of the plasma-modified solutions show another peak at Ex-Em of 360–446 nm (peak II). We tentatively attribute this peak to the formation of additional acid moieties in the solutions after PEPT.^[53]

The observed EEM results are likely directly related to the acidity of the solutions, because a pH change is known to affect the fluorescence yield as it can lead to fragmentation of organic molecules.^[54] Hence, pH measurements were also carried out to study possibly occurring plasma-induced acidity changes in the PLA solutions under various operational conditions and the obtained results are presented in Figure 6. The pH values of CHL could not be detected before and after PEPT. However, the pH of pure DMF was

found to decrease after plasma treatment (parameters: 5 min, 0.5 L min⁻¹, 2 kV) from 10.95 ± 0.27 for untreated DMF to 9.17 ± 0.63 for plasma-treated DMF. The pH of the binary solvent mixture of CHL:DMF (8:2 v/v) was also found to decrease after PEPT from 2.39 ± 0.18 to 1.58 ± 0.3 .

PEPT induced a considerable acidity in the plasma-treated PLA solutions. The acidity level was found to increase with increasing plasma treatment time, argon flow rate, and applied voltage (Figure 6a–c). The pH values considerably decrease (following an exponential trend) with increased plasma treatment time and argon flow rate, while the pH plotted against applied voltage follows a more linear trend. The PLA concentration had no significant effect on pH (Figure 6d).

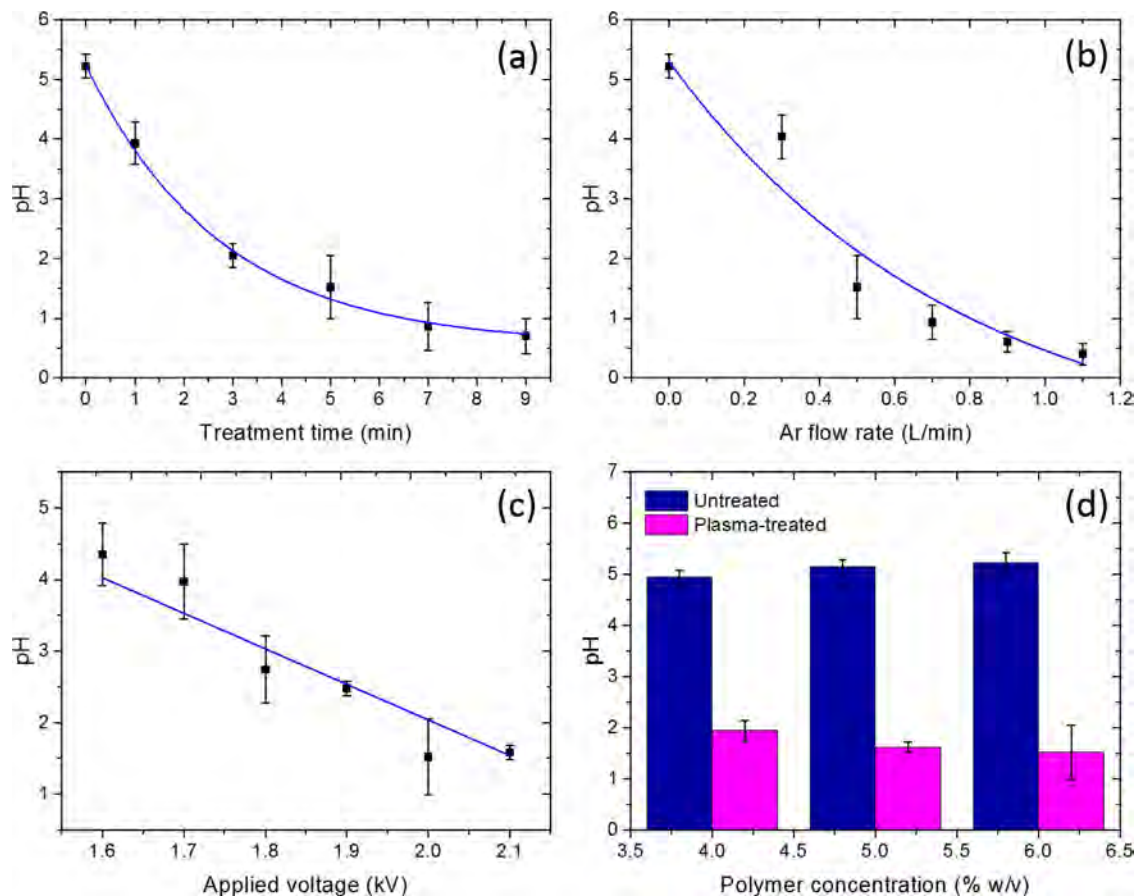


FIGURE 6 Obtained pH values for untreated and plasma-treated PLA solutions as a function of (a) treatment time (PEPT parameters: 2 kV, 0.5 L min^{-1} , 6% w/v), (b) argon flow rate (PEPT parameters: 5 min, 2 kV, 6% w/v), (c) applied voltage (PEPT parameters: 5 min, 0.5 L min^{-1} , 6% w/v), and (d) polymer concentration (PEPT parameters: 5 min, 2 kV, 0.5 L min^{-1})

Results from EEM spectroscopy for the same operational conditions as the ones shown in Figure 6 are also presented in Figure 7. From this figure, it can be clearly seen that with increasing plasma treatment time, argon gas flow rate, and applied voltage, the relative intensity of peak I decreases while the relative intensity of peak II increases. The presence of peak II in the plasma-treated PLA solutions is in good accordance with the increased solution acidity (observed with pH measurements). This peak may be attributed to some plasma-generated compounds in the solutions, which are formed through the decay of organic materials.^[55] Moreover, it has also been suggested that a change in fluorescent intensity with pH could be due to an alteration of the molecular orbital of the excitable electrons,^[56] which may occur as a consequence of ionization of organic molecules via PEPT.

Thus, we show the increased acidity induced in solutions after PEPT. However, it is also very important to determine whether the observed decrease in pH was due to the plasma-induced changes of the solvent molecules or if the PLA molecules also undergo chemical transformations during PEPT. For this, different liquid characterization techniques, such as UV-Vis, EPR, and NMR spectroscopy, were used.

UV-Vis spectroscopy was used to analyze the pure solvents, the binary solvent mixture and a 2% w/v PLA solution, before and after PEPT (as shown in Supporting Information, Figure S2). The absorbance spectra of all examined liquids showed a change after PEPT in the range 250–500 nm. In this wavelength range, the absorbance of the CHL:DMF mixture solvent and the PLA solution increased after PEPT, while also a shift towards higher wavelengths was observed for these solutions (Figure S2b). These effects can be attributed to changes occurring in the polarity of the solutions,^[57] in agreement with the induced acidity and conductivity.

4.3 | EPR analysis of the plasma-induced radicals

To gather more information on the source of the plasma-induced acidity in the pure organic solvents and also in the PLA solutions, an EPR study was also performed to investigate the plasma-generated radicals. Two different spin traps, DMPO, and PBN, were used to produce more stable and thus detectable radical adducts via reactions with

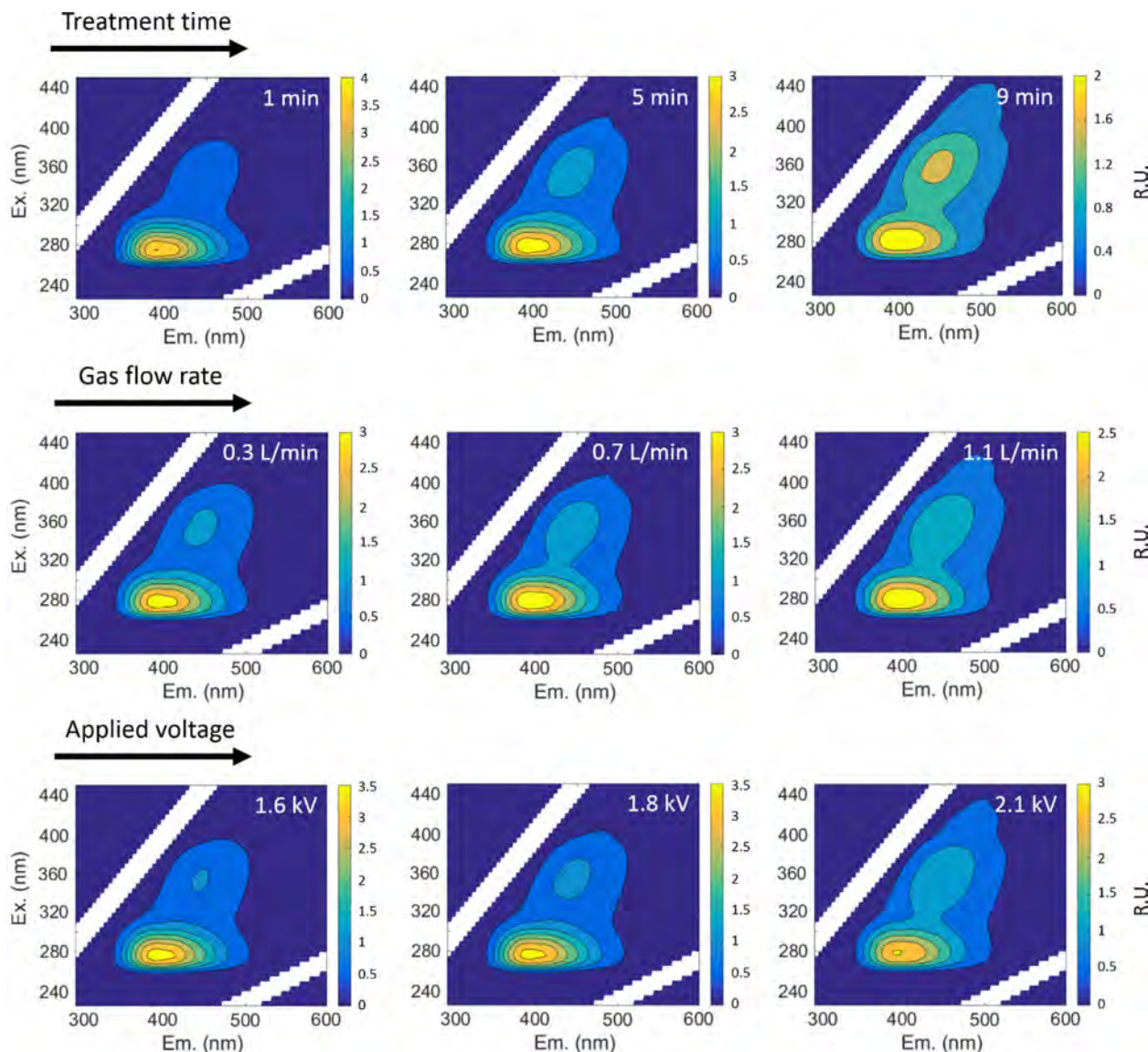


FIGURE 7 EEM spectra of the plasma-treated 6% w/v PLA solutions for various treatment times (top row; PEPT parameters: 2 kV, 0.5 L min^{-1}), argon flow rates (center row; PEPT parameters: 5 min, 2 kV), and applied voltage (bottom row; PEPT parameters: 5 min, 0.5 L min^{-1})

the otherwise too short-lived free radical species (see the Analysis section for details). We note that the same radicals were detected in the EPR spectra of plasma-treated PLA solutions with 2, 4, and 6% w/v PLA concentrations, except that their amount decreased as the concentration of PLA increased (not shown). The 2% w/v PLA concentration was therefore chosen for EPR analysis, albeit still resulting in a relatively weak spectrum. It is noteworthy to mention that the untreated solutions containing the spin traps only show EPR peaks with very low intensities which do not exceed the noise level of the EPR spectrometer. The assignment of the most prominent radical adducts (both nature and percentage) was based on the best simulation fitting.

The simulated EPR spectrum of the radical adducts with DMPO in plasma-treated CHL, DMF, the binary solvent

mixture, are presented in Figure 8a–c, respectively. The experimental and simulated EPR spectra of 2% w/v PLA solution is shown in Figure S3. Additionally, the total radical concentration as well as the relative concentration of the different DMPO-trapped radical adducts are presented in Table 1.

The EPR spectrum of plasma-treated CHL with DMPO, shown in Figure 8a, was composed of four components. These were the radical adducts DMPO-H, DMPO- CHCl_2 , and DMPO- CCl_3 , which were formed from the solvent itself, and an additional nitroxide adduct ($a_N = 1.42 \text{ mT}$), which was possibly a degradation product of DMPO.^[31]

The EPR spectrum of plasma-treated DMF using DMPO as spin trap reagent is shown in Figure 8b. This spectrum was composed of DMPO-H, DMPO- CH_3 , DMPO-CHO/CON(CH_3)₂,

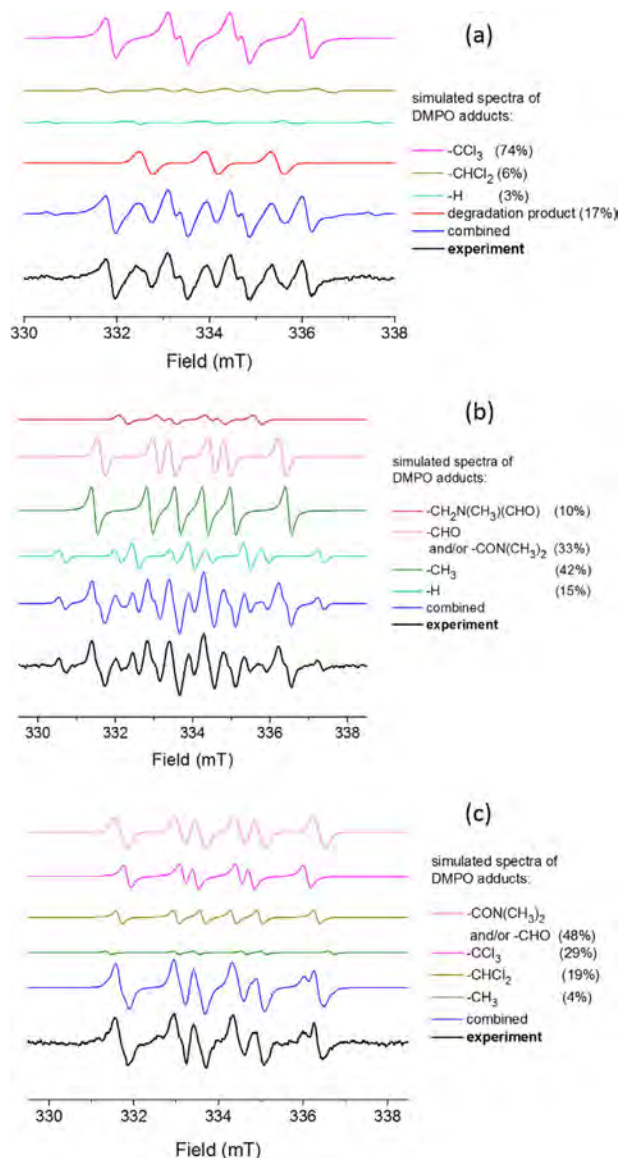


FIGURE 8 DMPO adducts in plasma-treated (a) CHL (Adducts: DMPO- CCl_3 [$a_N = 1.33$ mT, $a_H = 1.57$ mT]; DMPO- CHCl_2 [$a_N = 1.40$ mT, $a_H = 1.95$ mT]; DMPO-H [$a_N = 1.63$ mT, $a_H = 1.83$ mT ($\times 2$)]; unidentified, possibly a nitroxide degradation product of DMPO [$a_N = 1.42$ mT]), (b) DMF (Adducts: DMPO- $\text{CH}_2\text{N}(\text{CH}_3)(\text{CHO})$ [CHO] [$a_N = 1.26$ mT, $a_H = 0.96$ mT]; DMPO- $\text{CHO}/\text{-CON}(\text{CH}_3)_2$ [$a_N = 1.43$ mT, $a_H = 1.81$ mT]; DMPO- CH_3 [$a_N = 1.43$ mT, $a_H = 2.14$ mT]; DMPO-H [$a_N = 1.44$ mT, $a_H = 1.90$ mT ($\times 2$)]), and (c) CHL:DMF (8:2 v/v) (Adducts: DMPO- $\text{CHO}/\text{-CON}(\text{CH}_3)_2$ [$a_N = 1.41$ mT, $a_H = 1.86$ mT]; DMPO- CCl_3 [$a_N = 1.32$ mT, $a_H = 1.61$ mT]; DMPO- CHCl_2 [$a_N = 1.35$ mT, $a_H = 1.97$ mT]; DMPO- CH_3 [$a_N = 1.55$ mT, $a_H = 2.07$ mT])

and DMPO- $\text{CH}_2\text{N}(\text{CH}_3)(\text{CHO})$ adducts, which were formed from pure DMF during PEPT.

The PEPT of the DMPO solution in the binary solvent mixture (Figure 8c) resulted in the production of CH_3 , CHCl_2 , CCl_3 , and $\text{CHO}/\text{CON}(\text{CH}_3)_2$ radicals. This observation indicates that in the solvent mixture, both solvents undergo fragmentation via reactions with the generated plasma species.

Figure S3 illustrates the DMPO adducts in the plasma-treated 2% w/v PLA solution. This figure reveals that the presence of PLA in the binary solvent mixture does not change the nature of the trapped radicals, in agreement with the previously obtained OES results (see above, Figure 3). However, the data in Table 1 and Figure S3 clearly show that the total radical amount strongly decreases with the presence of PLA in the solution. Two possibilities could be considered for these observations: (1) the increased viscosity of the solution with adding PLA, leading to hindered mass transfer and hence slower spin trapping; (2) possible interactions of the radicals with the dissolved PLA molecules. Interestingly, there was a decrease in relative amount of one of the radical adducts: DMPO- $\text{CHO}/\text{CON}(\text{CH}_3)_2$ (Table 1). This may be due to the fast(er) interaction of these radicals with the dissolved PLA molecules. The same effect was also observed when PBN was used as a spin trap (see below).

Similar to DMPO, the formed radical adducts in plasma-treated CHL and DMF with PBN were those formed from the solvents upon PEPT (Figures 9a and 9b).

Besides these adducts, an additional unidentified PBN-adduct was also detected as shown in Figure 9b, which was possibly PBN- $\text{CON}(\text{CH}_3)_2$ or PBN- $\text{N}(\text{CH}_3)_2$. As previously mentioned, these radicals were most likely formed from the DMF molecules upon PEPT.

The simulated EPR spectra of the plasma-generated radicals in the CHL:DMF (8:2 v/v) mixture and in the 2% w/v PLA solution are presented in Figure 9c and Figure S4, respectively. They show the presence of the CHCl_2 , $\text{CH}_2\text{N}(\text{CH}_3)(\text{CHO})$, COH , and CH_3 radicals in both liquids, which are with the exception of CCl_3 exactly the same radicals as the ones which have been detected with DMPO. Similarly, the total amount of radicals detected with PBN strongly decreased when PLA was added to the solvent mixture (Table 1). Thus, as seen from the results of the EPR analysis, the solvent indeed underwent chemical transformations during PEPT, potentially leading to formation of new chemical compounds, which can be responsible for the observed pH changes.

4.4 | Analysis of the aqueous extracts

The EPR data have revealed that the solvents underwent chemical transformations during PEPT, potentially leading to formation of new chemical compounds, which can be responsible for the pH changes. With CHL and DMF present in the solvent mixture, it can be hypothesized that a possible PEPT product leading to decreased pH is hydrochloric acid (HCl). To confirm this hypothesis, we performed qualitative detection of the chloride anions. Untreated and plasma-treated 2% w/v PLA solutions were mixed with 4 mL H_2O . After 10 min, 0.5 mL of the aqueous phase was separated. Then, 0.05 mL of a 2M solution of AgNO_3 in H_2O was added to the collected aqueous phase. A rapid formation of the white

TABLE 1 The spin adducts of DMPO and PBN spin traps formed in the plasma-treated CHL, DMF, the CHL:DMF (8:2 v/v) mixture, and the 2% w/v PLA solution in the CHL:DMF mixture

Spin trap reagent	Solvent	Total adducts concentration (μM)	Radical adduct	Relative amount (%)
DMPO	CHL	57	-H	3
			-CHCl ₂	6
			-CCl ₃	74
			Degradation product	17
	DMF	48	-H	15
			-CH ₃	42
			-CHO/-CON(CH ₃) ₂	33
			-CH ₂ N(CH ₃)(CHO)	10
	CHL:DMF (8:2 v/v)	25	-CH ₃	4
			-CHCl ₂	19
			-CCl ₃	29
			-CHO/-CON(CH ₃) ₂	48
2% PLA solution	12	-CH ₃	16	
		-CHCl ₂	32	
		-CCl ₃	32	
		-CHO/-CON(CH ₃) ₂	20	
PBN	CHL	20	-CCl ₃	48
			-CHCl ₂	52
	DMF	41	-H	10
			Unidentified	32
			-CH ₃ /-CHO/ -CH ₂ N(CH ₃)(CHO)	58
	CHL:DMF (8:2 v/v)	32	-CHCl ₂	57
			-CH ₃ /-CHO/-CH ₂ N(CH ₃)(CHO)	43
			-CHCl ₂	66
	2% PLA solution	11	-CH ₃ /-CHO/ -CH ₂ N(CH ₃)(CHO)	34

precipitate (AgCl) was observed for the plasma-treated PLA solution, while no precipitation was seen for the untreated PLA solution. The same test was performed for untreated and plasma-treated pure CHL, DMF, and their binary mixture. In this case, precipitation only occurred for the plasma-treated binary mixture and not for the plasma-treated pure solvents. These observations suggest that an ionic polar compound with the Cl⁻ anion is produced by PEPT only when CHL and DMF are both present in the treated liquid. The pH measurements of the aqueous extracts showed that the pH has decreased from 6.69 and 6.81 for the untreated binary solvent mixture and the 2% w/v PLA solution, respectively, to 2.45 and 2.63 for the corresponding plasma-treated samples. No change was observed when the pure solvents were used. This decrease of pH is consistent with the formation of Cl⁻ under those conditions. Thus, we conclude that the plasma-induced species generated in the solvent mixture was HCl. In previous

work, we also suggested the possible formation of HNO₃ via PEPT as a result of the presence of DMF in the polymer solutions. Therefore a nitrate/nitrite colorimetric assay was performed (Assay kit-Cayman Chemical). For this assay, 80 μL of Assay Buffer was added to 80 μL of dilute plasma-treated samples (1:1). Then, 20 μL of Enzyme Cofactor Mixture and 20 μL of Nitrate Reductase Mixture were added to each sample. The samples were covered and incubated at room temperature for 1 hour. Then, 100 μL of Griess Reagent R1, and immediately after that 100 μL of Griess Reagent R2 were added to each sample. The samples were kept for 10 min and after that the absorbance at 540 or 550 nm was recorded using a plate reader. Using the Griess test with reductase, a negligible peak was observed for the aqueous extract from the plasma-treated binary solvent mixture, however, neither HNO₃ nor HNO₂ were detected in the aqueous extract from the plasma-exposed PLA solutions.

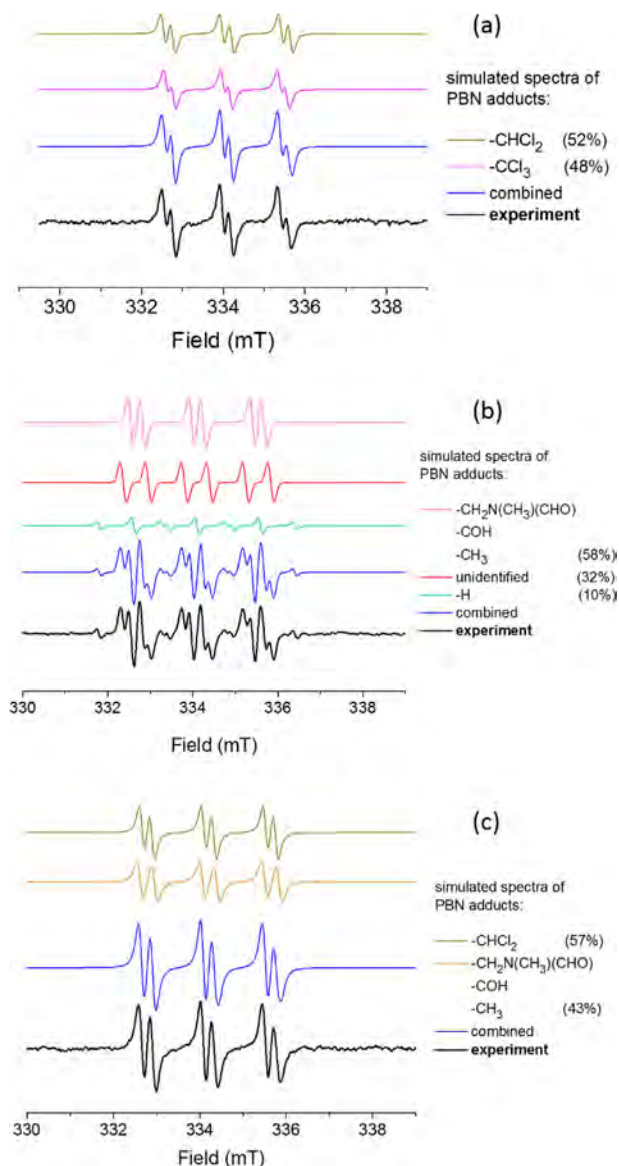


FIGURE 9 PBN adducts in plasma-treated (a) CHL (Adducts: PBN- CHCl_2 [$a_N = 1.43$ mT, $a_H = 0.22$ mT]; PBN- CCl_3 [$a_N = 1.39$ mT, $a_H = 0.17$ mT]), (b) DMF (Adducts: PBN- $\text{CH}_2\text{N}[\text{CH}_3][\text{CHO}]/\text{-COH}/\text{-CH}_3$ [$a_N = 1.43$ mT, $a_H = 0.3$ mT]; PBN-H [$a_N = 1.48$ mT, $a_H = 0.80$ mT (x2)]; unidentified [$a_N = 1.44$ mT, $a_H = 0.59$ mT]), and (c) CHL:DMF (8:2 v/v) (Adducts: PBN- CHCl_2 [$a_N = 1.43$ mT, $a_H = 0.23$ mT]; PBN- $\text{CH}_2\text{N}[\text{CH}_3][\text{CHO}]/\text{-COH}/\text{-CH}_3$ [$a_N = 1.45$ mT, $a_H = 0.33$ mT])

NMR analysis of the formed polar compounds was also performed. For this, the aqueous phase consisting of D_2O , similarly to extraction with H_2O , was added to the untreated and plasma-treated 2% w/v PLA solutions. The obtained D_2O extract of the PLA solution was used for ^1H and ^{13}C -NMR analysis (see Figure S5 and the related discussion in Supporting Information). The obtained aqueous phase extract thus consisted mostly of D_2O and DMF, together with a polar compound possibly formed during PEPT. The obtained NMR data showed that no new NMR signals were detected by either ^1H or ^{13}C -NMR analysis in the

aqueous phase extract, indicating the absence of organic cations. This, together with the result of the Cl^- anion detection, suggested that the acid formed in the solutions during PEPT was indeed HCl.

Additionally, ^1H -NMR analysis of PLA solution and the solvent mixture was performed. No new NMR peaks could be observed in the ^1H -NMR spectra (Figure S6 in Supporting Information). It could thus be tentatively concluded that, although the radicals detected by EPR in the solutions can interact to form new organic chemical products, these interactions must be minor due to absence of any significant amounts of these products.

4.5 | Morphology of the PLA nanofibers

The capability of PEPT to enhance the electrospinnability of various spinning solutions and consequently enhance the morphology of the resultant nanofibers has been previously demonstrated.^[6–8] In our case, it was concluded that mainly the large increases in viscosity and conductivity of the plasma-treated solutions play a role in enhancing the electrospinnability of PLA solutions. We showed that after PEPT (parameters: 5 min, 0.5 L min^{-1} , 2 kV) the remaining volume of a 10 mL 6% w/v PLA solution decreased from 10 to 8.4 mL.^[8] This was attributed to the solvent evaporation (mainly CHL) during PEPT and the plasma treatment itself. Hence, the final concentration of a starting 6% w/v PLA solution increased to 7.1% w/v after PEPT. As a result, plasma-treated PLA solutions were found to exhibit a higher viscosity than the pristine ones. We showed that the observed viscosity increase as such is not sufficient to enhance the PLA electrospinnability and that only the combination of increasing viscosity and conductivity resulted in PLA nanofibers with better morphology. We hypothesized that the increased solution conductivity plays a major role in the enhanced electrospinnability of the PLA solutions.

After conducting the pH measurements in this work, it was observed that the acidity of the PLA solutions decreased dramatically, as discussed above. We further conclude that mainly the plasma-induced formation of HCl is responsible for this increased acidity. Hence, the increased conductivity of the solutions after PEPT was likely due to the formed HCl. In other words, the improved electrospinnability of the PLA solutions was mainly due to the induction of HCl in the solutions during PEPT.

To confirm this hypothesis and to elucidate the role of the increased solution acidity, additional control experiments have been performed. These experiments were selected in such a way that they can help to determine whether the obtained enhancement in PLA nanofiber morphology is related to plasma-induced changes in the liquid chemistry, or to plasma-induced changes in the PLA polymer chains (or both).

TABLE 2 Performed control experiments in this work

Name	Description
CONTROL 1	PEPT was applied to CHL:DMF (8:2 v/v) mixture (5 min, 0.5 L min ⁻¹ , 2 kV). Then pristine PLA pellets were dissolved in the treated mixture to obtain a solution with 7.1% w/v concentration of PLA
CONTROL 2	PEPT was applied to CHL and DMF separately (5 min, 0.5 L min ⁻¹ , 2 kV). Then, a mixture of these treated CHL and DMF was prepared (6.4:2 v/v, to correspond to the solvent mixture after PEPT), and the pristine PLA pellets were dissolved in the treated solvent mixture to get a solution with 7.1% w/v concentration
CONTROL 3	A plasma-treated PLA solution was dried after PEPT at room temperature to obtain a plasma-treated PLA. This PLA was then dissolved in a pristine CHL:DMF mixture (6.4:2 v/v) to get a 7.1% w/v PLA solution
CONTROL 4	A pristine 7.1% PLA solution in a CHL:DMF mixture (6.4:2 v/v) was prepared. Then HCl was added gradually to the prepared solution to achieve the same pH as for the plasma-treated 6% PLA solution and then electrospinning was done with the prepared solution

Four different control PEPT experiments have been conducted (see description in Table 2). The resultant PLA solutions were subsequently used for electrospinning. To maintain the viscosity the same as for the plasma-treated PLA solution, the plasma-treated control samples were prepared with a fixed PLA concentration of 7.1% w/v. The SEM images of PLA nanofibers fabricated from an untreated PLA solution, a 6% w/v plasma-treated PLA solution (PEPT parameters: 5 min, 0.5 L min⁻¹, 2 kV) and the different control PLA solution samples selected in this work are shown in Figure 10. The results from pH, conductivity, and viscosity measurements for each investigated PLA solution are also listed in Table 3.

As seen from Figure 10 and Table 3, PEPT of the PLA solutions clearly had a positive effect on the electrospinnability of the nanofibers (compare Figures 10a and 10b).

In the first set of control experiments, either a mixture of solvent (Figure 10c) or individual solvents separately (Figure 10d) were plasma-treated, followed by dissolution of pristine PLA (to make 7.1% w/v). In both cases, the pH of the solution decreased while the conductivity and viscosity increased (Table 3). The data also show that the plasma-induced changes in physical properties were less pronounced for the sample CONTROL 2 compared to CONTROL 1 (Table 3). This resulted in the presence of more beads along the PLA nanofibers. Importantly, although the PLA nanofibers morphology for the sample CONTROL 1 was much better than for the pristine PLA, small beads along the nanofibers were still present. Comparing the nanofibers shown in Figure 10c and 10d, it is clearly seen that a treated binary solvent mixture has a better effect on PLA electrospinnability than a binary mixture from separately-treated solvents.

However, the most important discovery is that in both of these cases the nanofiber morphology was not as good (i.e., bead-free) as seen when PLA was plasma-treated together with the solvents (Figure 10b). This strongly suggests that presence of PLA molecules in the binary solvent mixture during PEPT lead to a more enhanced morphology.

Additionally, the plasma-treated PLA was dried from plasma-treated solvents and re-dissolved in an untreated solvent mixture. The electrospinning of this solution also resulted in nanofibers with small beads, as shown in Figure 10e.

According to the obtained results it can be concluded that the plasma-induced enhanced acidity, and as a result, the enhanced electrical conductivity (due to the presence of HCl) play a key role in determining the final electrospinnability of PLA solutions. Only when the acidity (and conductivity) is sufficiently enhanced, nicely elongated PLA nanofibers without the presence of beads can be attained. However, it may appear that addition of HCl to the untreated PLA solution will yield similar nanofibers as obtained for the plasma-treated PLA solution. To investigate this, we also added HCl to an untreated 7.1% w/v PLA solution to increase the acidity to the values obtained under PEPT conditions. The resulting nanofibers (Figure 10f) clearly illustrate that, unlike the uniform and bead-free PLA nanofibers obtained from the plasma-treated solution, the addition of HCl still leads to the formation of beads and a certain degree of non-uniformity along the fibers. In addition, the mean fiber diameter of the sample with added HCl was smaller (180 ± 83 nm) than that of the plasma-treated sample (370 ± 48 nm). At the same time, the physical properties (conductivity, viscosity, pH) of these two solutions had very similar values (Table 3). Therefore, it is possible that the plasma also affects the PLA polymer chains in the solution, which in turn also can affect the final electrospinnability behavior. Thus, the direct treatment of a PLA solution results in the lowest pH (and highest conductivity) and leads to the generation of bead-free, continuous, uniform, and thin PLA nanofibers.

4.6 | XPS analysis of the PLA nanofibers

To study the effects of PEPT on the surface chemical composition of the resultant PLA nanofibers, XPS measurements were carried out with untreated, plasma-treated, and also the control samples. The XPS survey spectra of all

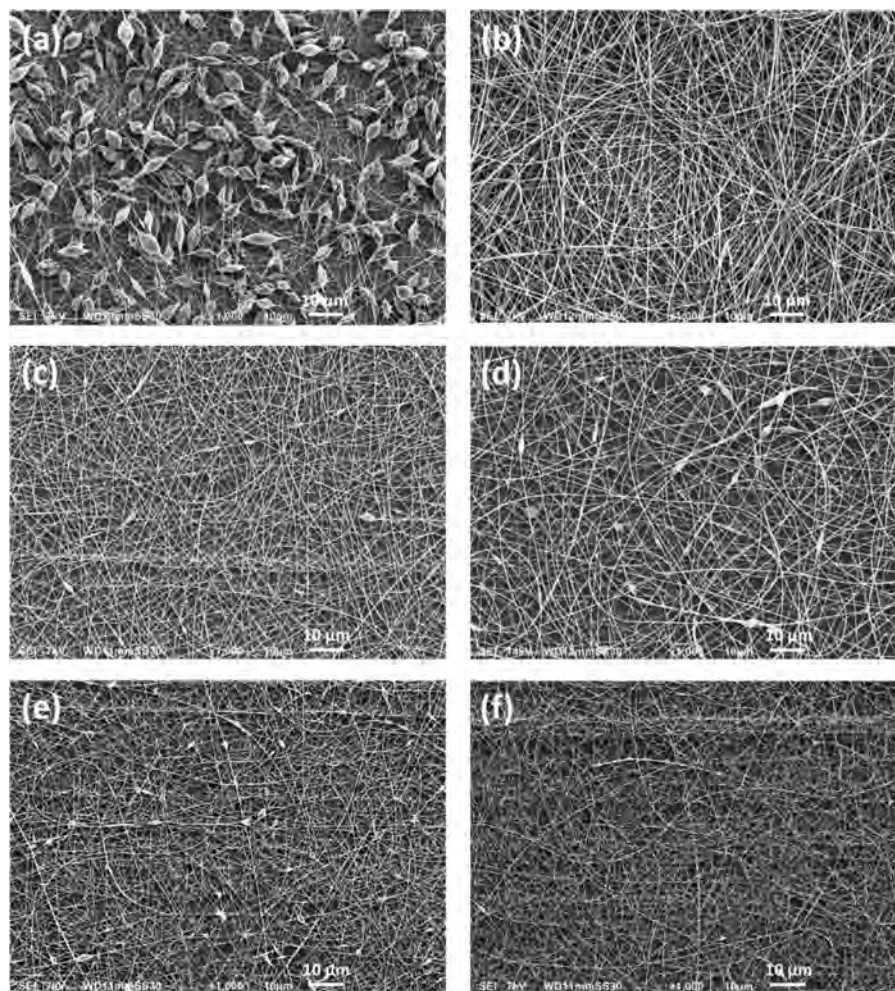


FIGURE 10 SEM images of electrospun PLA nanofibers fabricated from (a) an untreated PLA solution, (b) a plasma-treated 6% w/v PLA solution (PEPT parameters: 5 min, 0.5 L min^{-1} , 2 kV), (c) CONTROL 1, (d) CONTROL 2, (e) CONTROL 3, and (f) CONTROL 4

investigated samples show only carbon and oxygen peaks from which the O/C ratios were determined and listed in Table 4. The electronic C1s core level was also analyzed with high resolution and numerically fitted with Gaussian–Lorentzian functions. The C1s region was found to consist of three well resolved peaks at the binding energies 284.96, 286.88, and 288.95 eV, which can be assigned to C–C/C–H, C–O, and O–C=O groups, respectively (see Figure S7).

Table 4 demonstrates that after PEPT the surface oxygen content of the PLA nanofibers slightly increases, except for the sample CONTROL 4, where a more pronounced increase is observed. The samples CONTROL 1 and CONTROL 2 had a similar O/C ratio, meaning that treating the binary solvent mixture, and treating the CHL and DMF separately with subsequent mixing leads to the same final chemical composition of the electrospun PLA nanofibers. The

TABLE 3 Conductivity, viscosity, and pH values of an untreated PLA solution, a plasma-treated 6% w/v PLA solution (PEPT parameters: 5 min, 0.5 L min^{-1} , 2 kV), and the control samples

Solution	PLA concentration (% w/v)	pH	Conductivity ($\mu\text{S cm}^{-1}$)	Viscosity (cP)
Untreated PLA solution	6	5.22 ± 0.20	1.23 ± 1.30	87.72 ± 5.46
Treated PLA solution	7.1	1.52 ± 0.53	29.73 ± 1.70	146.16 ± 7.01
CONTROL 1	7.1	1.52 ± 0.61	32.93 ± 1.20	134.21 ± 5.40
CONTROL 2	7.1	3.12 ± 0.40	10.64 ± 1.45	150.75 ± 6.10
CONTROL 3	7.1	3.52 ± 0.50	7.58 ± 1.40	139.86 ± 7.50
CONTROL 4	7.1	2.64 ± 0.40	21.73 ± 1.50	129.90 ± 6.00

TABLE 4 XPS results of PLA nanofibers prepared from an untreated PLA solution, a plasma-treated 6% w/v PLA solution (PEPT parameters: 5 min, 0.5 L min⁻¹, 2 kV), and the control samples

Precursor	O/C ratio	Relative area (%)		
		C—C/C—H 284.96 eV	C—O 286.88 eV	O—C=O 288.95 eV
Untreated PLA solution	0.66	36.63	32.18	31.19
Treated PLA solution	0.69	35.68	32.21	32.11
CONTROL 1	0.70	37.51	28.96	33.53
CONTROL 2	0.70	37.23	28.64	34.13
CONTROL 3	0.70	37.88	28.32	33.80
CONTROL 4	0.76	34.54	31.25	34.21

chemical composition of PLA nanofibers electrospun from the sample CONTROL 3 also illustrated that the presence of plasma-treated PLA molecules in an untreated binary solvent mixture leads to a similar chemical composition as for CONTROL 1 and 2. The slightly higher O/C ratio for the control samples 1–3 is mainly due to a relative increase in O—C=O bonds combined with a relative decrease in C—O groups. When examining the surface chemical composition of the control samples 1–3, one can see that a similar O/C ratio is obtained. However, some minor changes in the type of functional groups can be seen. For example for the PLA nanofibers electrospun from a plasma-treated PLA solution, only a very small relative increase in O—C=O bonds can be observed with no relative decrease in C—O bonds.

Comparing the plasma-treated sample with the sample CONTROL 4 shows that the presence of HCl in the untreated PLA solution has a noticeably higher oxidation/degradation effect than the plasma-induced HCl in the treated solution. Most probably, the added HCl in the untreated PLA solution causes hydrolytic degradation effects via chain scission of carbonyl ester bond in the polymer backbone.^[58] This can also explain the observed morphological difference between the plasma-treated sample and the sample CONTROL 4 (Figures 10b and 10f). Based on XPS analysis, it can be concluded that the chemical composition of PLA is most preserved when the plasma-treated PLA solution is electrospun. This makes the developed PEPT method highly beneficial, as the preservation of the chemical composition of the original polymer is crucial in most applications.

5 | CONCLUSION

In this work, we aimed to gain deeper understanding of the plasma-enhanced electrospinnability of PLA solutions. We investigated PEPT-induced chemical and physico-chemical changes in organic solutions of PLA, used for the enhanced production of electrospun fibers. Pure solvents (CHL, DMF) and a mixture of CHL and DMF (with and without added PLA) were studied. The investigation included EEM, EPR,

UV–Vis absorption, and NMR analyses, as well as measurements of viscosity, pH, and conductivity of the plasma-treated liquids. These techniques were used to determine the chemical changes to the solvent molecules, and the nature of species which lead to the enhanced electrospinning. Both pure solvents (CHL, DMF) and a mixture of CHL and DMF (with and without added PLA) were studied in this work. Additionally, the PEPT-induced effects on the morphology and chemistry of resultant electrospun PLA nanofibers was also addressed.


OES measurements of the plasma jet afterglow generated inside the different liquids were used to gain insights into the plasma-generated species in the PLA solutions as well as in the solvent mixture. Radical species formed in the pure solvents, the solvent mixture and the PLA solution upon PEPT were also detected by EPR. Using EEM spectroscopy, in conjunction with the aqueous extraction method and ¹H and ¹³C-NMR, we propose that the main induced species responsible for the increased conductivity was hydrochloric acid (HCl). Morphological SEM studies of electrospun PLA nanofibers illustrated that a complete morphology enhancement only occurs when both PLA and solvent molecules were exposed to PEPT. No large changes in the surface chemical composition of the electrospun PLA nanofibers were observed in this case. Thus, the studied PEPT of polymer solutions is an indispensable tool in enhancing the electrospinnability of different polymers.

ACKNOWLEDGMENTS

This research was supported by a research grant (G.0379.15N) from the Research Foundation Flanders (FWO) and has also received funding from the European Research Council (ERC) under the European Union's Seventh Framework Program (FP/2007-2013)/ERC Grant Agreement n. 335929 (PLASMATS). Yury Gorbanev thanks the European Marie Skłodowska-Curie Individual Fellowship “LTPAM” within Horizon2020 (grant no. 657304) for supporting his work. The authors would like to thank Kenn Foubert (Department of Pharmaceutical Sciences, University

of Antwerp), Angela Privat-Maldonado (Research group PLASMANT, Department of Chemistry, University of Antwerp) and Sylvia Dewilde (Department of Biomedical Sciences, University of Antwerp) for their help with the equipment. Moreover, the authors would like to thank Prof. Dr. Freddy Callens (Department of Solid State Sciences, Ghent University) for his thoughtful comments on the EPR measurements.

ORCID

Fatemeh Rezaei  <http://orcid.org/0000-0002-3316-9836>

REFERENCES

- [1] X. Lu, G. V. Naidis, M. Laroussi, S. Reuter, D. B. Graves, K. Ostrikov, *Phys. Rep.* **2016**, *630*, 1.
- [2] Y. Gorbanev, D. Leifert, A. Studer, D. O'Connell, V. Chechik, *Chem. Commun.* **2017**, *53*, 3685.
- [3] I. Adamovich, S. D. Baalrud, A. P. J. Bogaerts Bruggeman, M. Cappelli, V. Colombo, U. Czarnetzki, U. Ebert, J. G. Eden, P. Favia, D. B. Graves, S. Hamaguchi, G. Hieftje, M. Hori, I. D. Kaganovich, U. Kortshagen, M. J. Kushner, N. J. Mason, S. Mazouffre, S. Mededovic Thagard, H.-R. Metelmann, A. Mizuno, E. Moreau, A. B. Murphy, B. A. Niemira, G. S. Oehrlein, Z. Lj. Petrovic, L. C. Pitchford, Y.-K. Pu, S. Rauf, O. Sakai, S. Samukawa, S. Starikovskaia, J. Tennyson, K. Terashima, M. M. Turner, M. C. M. van de Sanden, A. Vardelle, *J. Phys. D: Appl. Phys.* **2017**, *50*, 323001.
- [4] P. Bruggeman, C. Leys, *J. Phys. D: Appl. Phys.* **2009**, *42*, 53001.
- [5] F. Rezaei, N. De Geyter, R. Morent, presented at 2016 IEEE Int. Conf. Plasma Sci., Pre-electrospinning polymer solution treatment by atmospheric-pressure argon plasma jet, Canada, 2016.
- [6] Q. Shi, N. Vitichuli, J. Nowak, Z. Lin, B. Guo, M. McCord, M. Bourham, X. Zhang, *J. Polym. Sci. B: Polym. Phys.* **2011**, *49*, 115.
- [7] V. Colombo, D. Fabiani, M. L. Focarete, M. Gherardi, C. Gualandi, R. Laurita, M. Zaccaria, *Plasma Process. Polym.* **2014**, *11*, 247.
- [8] F. Rezaei, A. Nikiforov, R. Morent, N. De Geyter, *Sci. Rep.* **2018**, *8*, 2241.
- [9] R. Laurita, M. Zaccaria, M. Gherardi, D. Fabiani, A. Merlettoni, A. Pollicino, M. L. Focarete, V. Colombo, *Plasma Process. Polym.* **2016**, *13*, 124.
- [10] D. Annur, Z. K. Wang, J. D. Liao, C. Kuo, *Biomacromolecules* **2015**, *16*, 3248.
- [11] J. Venugopal, S. Ramakrishna, *Appl. Biochem. Biotechnol.* **2005**, *125*, 147.
- [12] S. Agarwal, J. H. Wendorff, A. Greiner, *Polymer (Guildf)*. **2008**, *49*, 5603.
- [13] S. Homaeigohar, M. Elbahri, *Materials (Basel)*. **2014**, *7*, 1017.
- [14] N. Bhardwaj, S. C. Kundu, *Biotechnol. Adv.* **2010**, *28*, 325.
- [15] F. Ko, *Nanoeng. Nanofibrous Mater.* **2004**, *1*.
- [16] V. Pillay, C. Dott, Y. E. Choonara, C. Tyagi, L. Tomar, P. Kumar, L. C. du Toit, V. M. K. Ndesendo, *J. Nanomater.* **2013**, *2013*.
- [17] M. S. Khil, D. I. Cha, H. Y. Kim, I. S. Kim, N. Bhattarai, *J. Biomed. Mater. Res. B: Appl. Biomater.* **2003**, *67*, 675.
- [18] E. R. Kenawy, F. I. Abdel-Hay, M. H. El-Newehy, G. E. Wnek, *Mater. Sci. Eng. A* **2007**, *459*, 390.
- [19] J. E. Oliveira, L. H. C. Mattoso, W. J. Orts, E. S. Medeiros, *Adv. Mater. Sci. Eng.* **2013**, *2013*, 1.
- [20] C. Z. Li, C. Wang, *One-Dimensional Nanostructures*, Springer, Berlin Heidelberg **2013**.
- [21] S. F. Dehghan, F. Golbabaie, B. Maddah, M. Latifi, H. Pezeshk, M. Hasanzadeh, F. Akbar-Khanzadeh, *J. Air Waste Manag. Assoc.* **2016**, *66*, 912.
- [22] V. Beachley, X. Wen, *Mater. Sci. Eng. C* **2009**, *29*, 663.
- [23] A. K. Moghe, R. Hufenus, S. M. Hudson, B. S. Gupta, *Polymer (Guildf)*. **2009**, *50*, 3311.
- [24] X. H. Qin, E. L. Yang, N. Li, S. Y. Wang, *J. Appl. Polym. Sci.* **2007**, *103*, 3865.
- [25] W. Klairutsamee, P. Supaphol, I. Jangchud, *J. Appl. Polym. Sci.* **2015**, *132*, 42716.
- [26] X. Wang, C. Pellerin, C. G. Bazuin, *Macromolecules* **2016**, *49*, 891.
- [27] P. Wang, National Institute of Health, Center for Scientific Review, Evaluation of Novel Tissue Scaffolds for Implantation, **2010**. Available at: <https://engineering.wustl.edu/current-students/student-services/ecc/Documents/Wang.pdf>
- [28] Q. Shi, N. Vitichuli, J. Nowak, J. M. Caldwell, F. Breidt, M. Bourham, X. Zhang, M. McCord, *Eur. Polym. J.* **2011**, *47*, 1402.
- [29] R. P. Pawar, S. U. Tekale, S. U. Shisodia, J. T. Totre, A. J. Domb, *Rec. Pat. Regen. Med.* **2014**, *4*, 40.
- [30] K. Murphy, C. Stedmon, D. Graeber, R. Bro, *Anal. Methods* **2013**, *5*, 6557.
- [31] NIEHS Spin Trap Database. Available at: <https://tools.niehs.nih.gov/stdb/>
- [32] A. Sarani, A. Nikiforov, C. Leys, *Phys. Plasmas* **2010**, *17*, 63504.
- [33] Q. Xiong, A. Y. Nikiforov, X. P. Lu, C. Leys, *J. Phys. D: Appl. Phys.* **2010**, *43*, 415201.
- [34] F. Rezaei, M. Abbasi-Firouzjah, B. Shokri, *J. Phys. D: Appl. Phys.* **2014**, *47*, 85401.
- [35] G. Alcouffe, M. Cavarroc, G. Cernogora, F. Ouni, A. Jolly, L. Boufendi, C. Szopa, *Plasma Sources Sci. Technol.* **2009**, *19*, 15008.
- [36] S. J. Kim, T. H. Chung, S. H. Bae, S. H. Leem, *Appl. Phys. Lett.* **2009**, *94*, 141502.
- [37] D. B. Luo, Y. X. Duan, Y. He, B. Gao, *Sci. Rep.* **2014**, *4*, 7451.
- [38] A. Chingsungnoen, J. I. B. Wilson, V. Amornkitbamrung, C. Thomas, T. Burinprakhon, *Plasma Sources Sci. Technol.* **2007**, *16*, 434.
- [39] C. H. Su, C. Y. Chang, *Mater. Trans.* **2008**, *49*, 1380.
- [40] A. Mohanta, B. Lanfant, M. Asfaha, M. Leparoux, *J. Phys. Conf. Ser.* **2017**, *825*, 12010.
- [41] J. H. Han, T. Y. Lee, J. B. Yoo, C.-Y. Park, T. Jung, J. M. Kim, S. G. Yu, W. Yi, *J. Vac. Sci. Technol. B: Microelectron. Nanom. Struct.* **2003**, *21*, 1720.
- [42] E. Thimsen, U. R. Kortshagen, E. S. Aydil, *J. Phys. D: Appl. Phys.* **2015**, *48*, 314004.
- [43] T. Ouerhani, R. Pflieger, W. Ben Messaoud, S. I. Nikitenko, *J. Phys. Chem B* **2015**, *119*, 15885.
- [44] S. F. Adams, E. A. Bogdanov, V. I. Demidov, M. E. Koepke, A. A. Kudryavtsev, J. M. Williamson, *Phys. Plasmas*. **2012**, *19*, 23510.
- [45] Z. Rašková, PhD Thesis, Brno University of Technology, **2006**.
- [46] S. A. Sell, P. S. Wolfe, K. Garg, J. M. McCool, I. A. Rodriguez, G. L. Bowlin, *Polymers* **2010**, *2*, 522.
- [47] C. P. Barnes, S. A. Sell, E. D. Boland, D. G. Simpson, G. L. Bowlin, *Adv. Drug. Deliv. Rev.* **2007**, *59*, 1413.
- [48] K. Jayaraman, M. Kotaki, Y. Zhang, X. Mo, S. Ramakrishna, *J. Nanosci. Nanotechnol.* **2004**, *4*, 52.
- [49] A. Yunus, PhD Thesis, University of Southampton, **2009**.

- [50] Á. Andrade-Eiroa, M. Canle, V. Cerdá, *Appl. Spectrosc. Rev.* **2013**, *48*, 77.
- [51] M. Gonsior, PhD Thesis, University of Otago, New Zealand, **2008**.
- [52] K. Appalaneni, PhD Thesis, University of Central Florida, **2013**.
- [53] W. Chen, P. Westerhoff, J. Leenheer, *Environ. Sci. Technol.* **2003**, *37*, 5701.
- [54] B. Matthews, A. Jones, N. Theodorou, A. Tudhope, *Mar. Chem.* **1996**, *55*, 317.
- [55] B. Teymouri, Master Thesis, University of Missouri-Columbia, **2007**.
- [56] N. Patel-Sorrentino, S. Mounier, J. Benaim, *Water Res.* **2002**, *36*, 2571.
- [57] M. Trivedi, *Org Chem Curr Res.* **2015**, *4*, 3.
- [58] C. S. H. Keles, A. Naylor, F. Clegg, *Polym. Degrad. Stab.* **2015**, *119*, 228.

SUPPORTING INFORMATION

Additional Supporting Information may be found online in the supporting information tab for this article.

How to cite this article: Rezaei F, Gorbanev Y, Chys M, et al. Investigation of plasma-induced chemistry in organic solutions for enhanced electrospun PLA nanofibers. *Plasma Process Polym.* 2018;**15**:e1700226.

<https://doi.org/10.1002/ppap.201700226>